

The ATA Offset Gregorian Antenna

David DeBoer
February 10, 2001

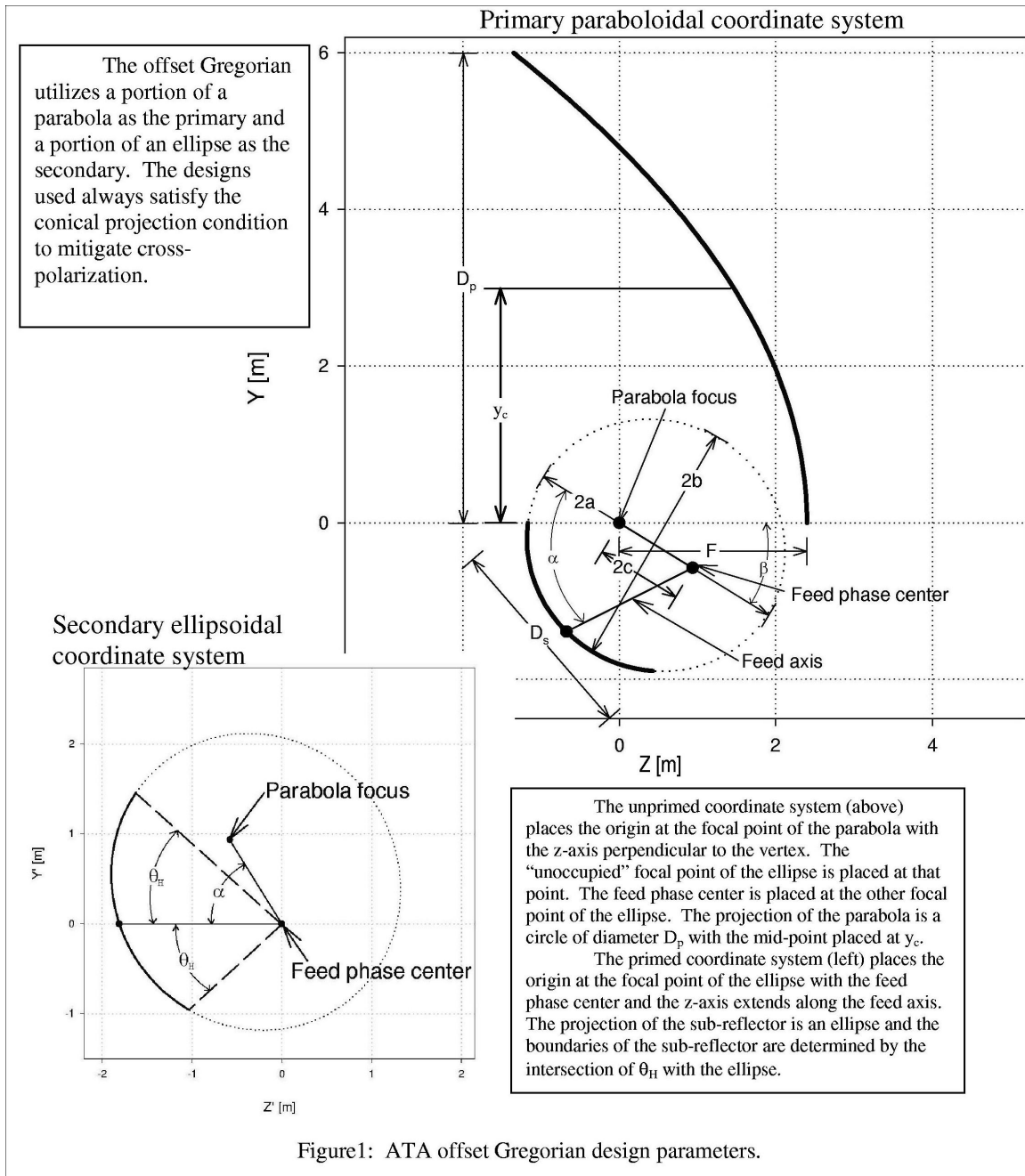
Abstract

This memo describes the detailed design of the Allen Telescope Array (ATA) offset Gregorian antenna, which will be a 6-meter antenna designed to operate from about 600 MHz to 11 GHz with a single tapered log-periodic feed. The strawman design for the array consists of about 350 such antennas, to provide about one hectare of physical collecting area, with a design figure-of-merit $A_e/T_{\text{sys}}=150 \text{ m}^2/\text{K}$. Based on the performance and mechanical constraints, a design with $0.40 \leq f/D \leq 0.45$ and $0.45 \leq y_c/D \leq 0.50$ is indicated.

Introduction

Given the advantages of a clear aperture antenna (greater effective area and lower sidelobes), an offset Gregorian antenna has been chosen as the ATA antenna design. The design constraints are the feed angle which yields a 12 dB edge taper based on the computer simulations of the log periodic feed (θ_H) and the Mizugutch condition on the optics (*i.e.* contours of constant E and H amplitudes in the reference plane are concentric) that nulls the inherent cross-polarization of most offset designs [1]-[4]. These constraints leave a relatively small parameter space for the detailed design. Another driving factor in the design is to produce a compact antenna to simplify the mount as much as possible and to provide appropriate curvature of the primary to provide stiffness.

A Gregorian antenna consists of a parabolic primary and an ellipsoidal secondary. In an offset design, non-symmetric portions of these conic sections are used in order to move the secondary and feed out of the primary aperture. The optics may still be characterized by the primary f/D ratio (focal length of the parent parabola over the projected diameter of the primary) and the eccentricity of the secondary. The distance separating the primary and secondary normal to the optical axis (characterized by the height of the primary mid-point, y_c) and the relative rotations of the feed and secondary are also required, as is the angle subtended by the feed pattern, θ_H , as mentioned above. Figure 1 shows the relevant quantities in the design. If these values are chosen correctly, the cross-polarization induced at one reflector is compensated at the second reflector. The rest of the analysis will assume this optimization has been implemented as described below.



Antenna Design Parameters

In order to more easily parameterize the design, we introduce two new variables which incorporate the quantities of interest in the design:

$$\xi = 2 \frac{f}{D} \tan\left(\frac{\theta_H}{2}\right)$$

$$\zeta = \frac{y_c/D}{f/D}$$

The eccentricity of the ellipse (e) and the angle that it makes with the optical axis (β) may be derived by solving a pair of transcendental equations:

$$e = \frac{\cos \beta \pm \sqrt{\cos^2 \beta + 4\xi^2 - 1}}{1 + 2\xi}$$

$$e = -\left[\frac{2 \sin \beta}{\zeta} - \cos \beta\right] \pm \sqrt{\left[\frac{2 \sin \beta}{\zeta} - \cos \beta\right]^2 - 1}$$

The signs are chosen to yield positive quantities. Figure 2 plots lines of constant ξ and ζ in the (e, β) plane, along with three lines of constant y_c/D , assuming $\theta_H = 42^\circ$. With a choice of ξ and ζ (i.e. f, D, y_c and θ_H), values for e and β may be computed or read from the chart. The orientation of the feed relative to the ellipse axis may then be calculated as

$$\tan\left(\frac{\alpha}{2}\right) = \frac{1+e}{1-e} \tan\left(\frac{\beta}{2}\right)$$

The final parameter is the scale of the ellipse, characterized by the interfocal distance, $2c$. This parameter may be iteratively applied to yield the desired sub-reflector size. Given the design constraints, the detailed analysis will be limited to be near the zero-separation curve ($y_c/D=0.5$, middle line of Figure 2) between $0.35 \leq f/D \leq 0.50$, which is indicated by the shaded region in the Figure 2.

Code has been implemented to produce these solutions and compute many of the other quantities of interest, e.g. the edge values for the reflectors, the surface area, etc. In addition this code provides output files for subsequent analysis, as will be discussed.

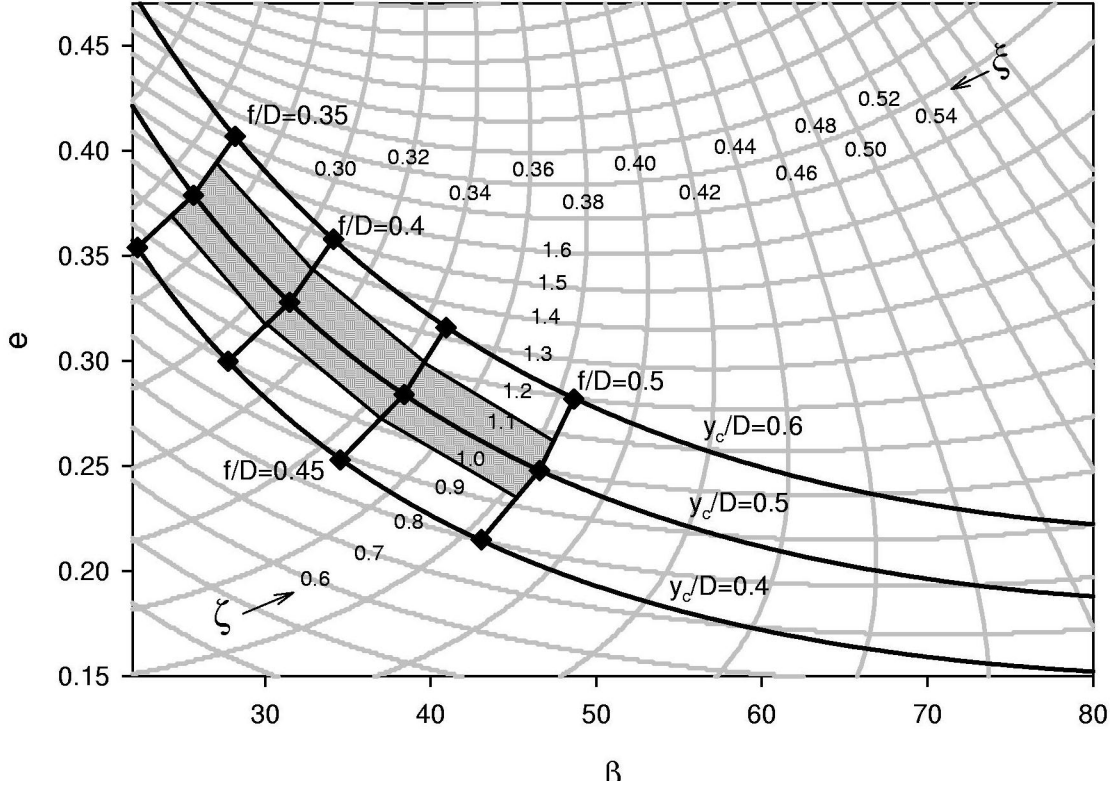


Figure 2: Design curves for offset Gregorian design with no net cross-polarization

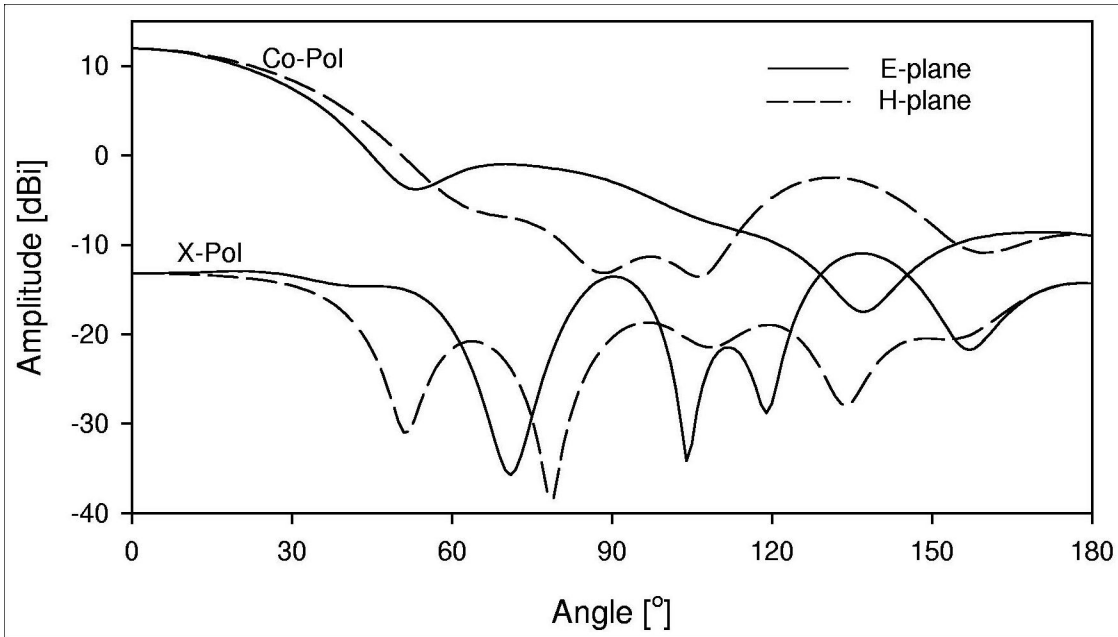


Figure 3: Feed amplitude patterns.

Feed Patterns

The feed design and patterns used in the full antenna analysis were derived via method of moments using software from Zeland, Inc. by Greg Engargiola. The amplitude patterns are shown in Figure 3. The 12-dB edge taper is found to occur at about $\theta_H = 42$ and roughly 80% of the power is contained within that contour.

The origin providing the relative phase is somewhat arbitrary, so the phase patterns have been translated to yield the in-focus version. Any defocusing will be done in the antenna analysis code. Figure 4 shows the original and modified phase patterns with different phase center origins. Note the distance adopted for this analysis was -33 cm from the original origin. This distance yields approximately equal and opposite curvature in the E and H planes. Note that least square fits to the phase patterns yield -25 cm for the E-plane and -44 cm for the H-plane, using the feed amplitude pattern as the weighting. This is however dependent on the weighting scheme used, and -33 cm seems to produce a good eyeball compromise.

Antenna Analysis

The code used for the analysis for the offset Gregorian design is a specially modified version of the Ohio State Numerical Electromagnetic Code for Reflector Antennas (NECREF) [5]. The modifications were necessary to be able to analyze this style of Gregorian offset and not all of the NECREF options are yet available to fully support the new version. The outputs are antenna patterns based on the Physical Optics (PO) analysis utilizing some diffraction analysis. It is unclear what diffraction analysis is supported on the sub-reflector with the new modifications, and I am still working with the vendor to ascertain this. Both in-focus and out-of-focus configurations have been analyzed. Table I summarizes the configurations and frequencies analyzed, as described later.

Additional code was written to integrate these patterns and provide various antenna parameters. The beam solid angle is given by

$$\Omega_A = \frac{1}{F_{\max}} \int_0^{2\pi} \int_0^\pi F(\theta, \varphi) \sin \theta d\theta d\varphi$$

where $F(\theta, \varphi)$ is the antenna power pattern. This may be written in several ways to accommodate symmetry and different griddings. One integration scheme is

$$\Omega_A = \frac{2}{F_{\max}} \int_{-\pi}^{\pi} \left\{ \int_0^{\pi/2} F(\theta, \varphi) d\varphi \right\} |\sin \theta| d\theta$$

$$\Omega_A = \frac{2}{F_{\max}} \int_{-\pi}^{\pi} \left\{ \sum_{j=0}^{N-1} \int_{j\pi/2N}^{(j+1)\pi/2N} F(\theta, \varphi) d\varphi \right\} |\sin \theta| d\theta$$

$$\Omega_A \approx \frac{2}{F_{\max}} \sum_{i=0}^{M-1} \sum_{j=0}^{N-1} \frac{1}{2} [F(\theta_i, \varphi_j) + F(\theta_i, \varphi_{j+1})] \Delta\varphi |\sin\theta_i| \Delta\theta$$

Different grids were also used, which do produce different answers, at least to the resolution achievable with the NECREF code. The directivity is then

$$G_o = 4\pi/\Omega_A$$

and the aperture efficiency is

$$\varepsilon_{ap} = \frac{G_o}{(\pi D / \lambda)^2}$$

where D is the diameter of the primary and λ is the wavelength of interest. Note that the primary is always taken as 6.096 m (20 ft) and the sub-reflector diameter is taken as 2.4 m, which is the geometric mean of the semi-major and semi-minor axes of the ellipse defined by the projection of the sub-reflector normal to the aperture.

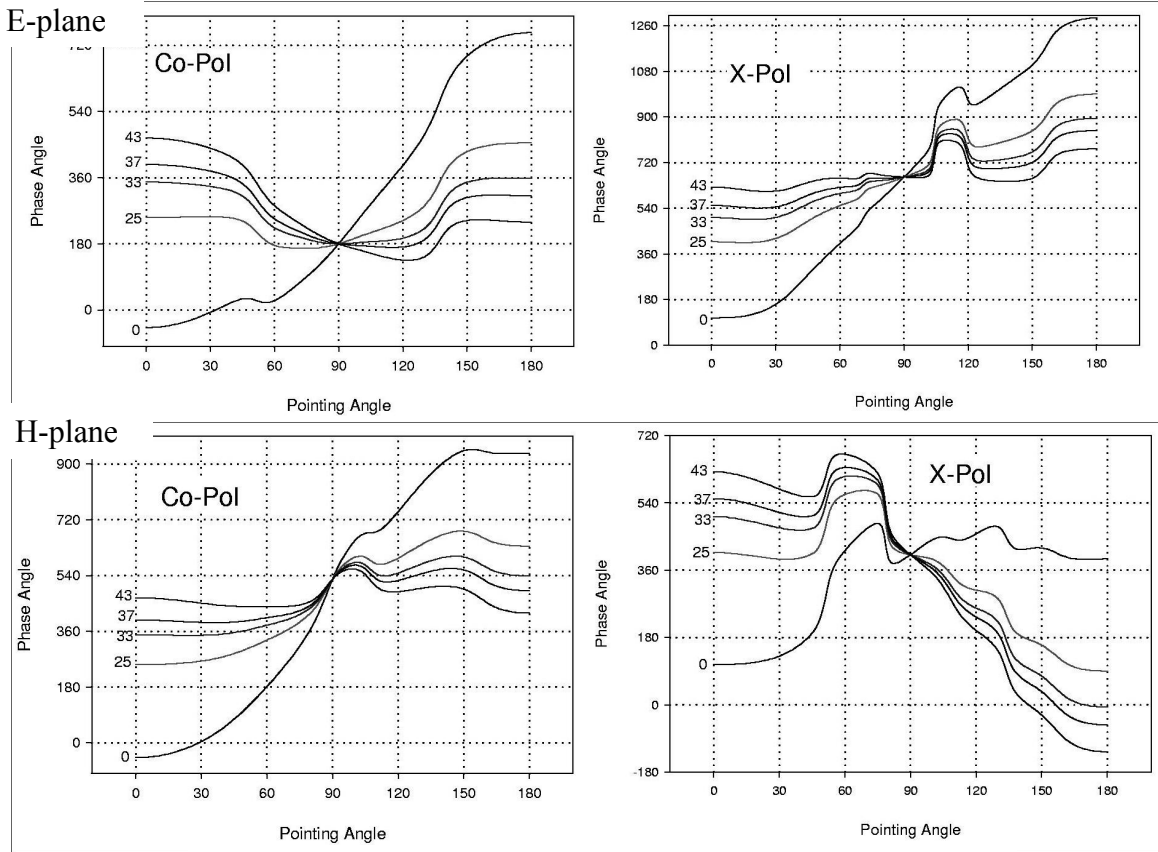


Figure 4: Feed phase patterns for various translations.

The results at 600MHz and 1 GHz are summarized in Table I. Columns 1-4 contain the input parameters and the remaining columns contain the derived data for two gridding options, one as described above (Grid 2) and another using $0 \leq \theta \leq 180$, $0 \leq \varphi \leq 180$

(Grid 1). The preferable solution of increasingly finer gridding to watch for asymptotic values was not performed due to memory limitations in the NECREF code. There is a time-consuming way around this, which may be performed at a later date if warranted. Note that the 3dB BW's for Grid 1 assume a symmetric pattern. The columns labeled “>10dBi” and “>0dBi” show the fraction of pattern on the sky (in per cent) that exceeds those magnitude limits, including the main beam.

Table I: Summary of antenna PO-GTD analysis

y_0/D	f/D	Freq [GHz]	Focus [cm]	Grid 1					Grid 2				
				G_0 [dBi]	ϵ_{ap} [%]	BW_{3dB} [°]	>10dBi [%]	>0dBi [%]	G_0 [dBi]	ϵ_{ap} [%]	BW_{3dB} [°]	>10dBi [%]	>0dBi [%]
0.45	0.35	0.6	-30	29.5	61	5.7	0.36	6.11	29.6	63	5.3	0.37	7.16
		1.0	0	34.0	62	3.6	0.23	2.31	34.2	65	3.4	0.21	1.97
			-30	33.6	56	3.5	0.33	6.24	33.7	58	3.2	0.31	6.61
	0.40	0.6	-30	29.5	60	5.6	0.32	5.06	29.3	59	5.5	0.36	6.62
		1.0	0	34.0	62	3.6	0.26	1.41	34.2	65	3.4	0.25	1.30
			-30	33.6	56	3.4	0.33	6.56	33.8	58	3.2	0.32	7.07
	0.45	0.6	-30	29.1	56	5.9	0.42	6.48	29.3	58	5.4	0.39	8.03
		1.0	0	34.1	63	3.5	0.22	1.83	34.2	65	3.4	0.22	1.56
			-30	33.7	58	3.3	0.31	5.90	33.8	59	3.1	0.31	6.47
	0.50	0.6	-30	29.5	61	5.6	0.40	5.23	29.6	62	5.3	0.38	7.42
		1.0	0	34.1	63	3.4	0.19	1.29	34.1	63	3.4	0.20	1.26
			-30	33.7	58	3.3	0.34	6.74	33.7	58	3.2	0.33	6.76
0.50	0.35	0.6	-30	29.3	59	5.86	0.36	6.70	29.6	62	5.3	0.34	7.75
		1.0	0	34.0	62	3.56	0.24	1.82	34.1	63	3.4	0.22	1.51
			-30	33.6	57	3.4	0.34	6.54	33.7	58	3.23	0.32	6.81
	0.40	0.6	-30	29.5	61	5.6	0.30	6.18	29.4	59	5.5	0.33	5.91
		1.0	0	34.0	62	3.5	0.22	1.56	34.2	65	3.4	0.20	0.98
			-30	33.6	56	3.4	0.32	6.22	33.7	58	3.2	0.29	5.13
	0.45	0.6	-30	29.0	54	6.0	0.43	6.30	29.2	57	5.5	0.35	6.39
		1.0	0	34.0	62	3.5	0.21	2.21	34.2	65	3.4	0.18	1.25
			-30	33.7	57	3.4	0.29	6.04	33.8	59	3.2	0.28	4.94
	0.50	0.6	-30	29.4	60	5.7	0.36	5.65	29.6	62	5.3	0.33	6.29
		1.0	0	34.1	63	3.5	0.14	1.44	34.2	65	3.4	0.14	0.86
			-30	33.7	58	3.3	0.30	6.23	33.8	59	3.2	0.27	5.21
0.55	0.35	0.6	-30	29.2	56	6.0	0.37	6.71	29.5	61	5.3	0.32	7.95
		1.0	0	34.0	62	3.5	0.21	1.55	34.1	63	3.4	0.21	1.41
			-30	33.7	58	3.4	0.33	7.14	33.8	58	3.2	0.31	7.29
	0.40	0.6	-30	29.5	61	5.6	0.30	6.31	29.5	60	5.4	0.32	8.37
		1.0	0	33.9	60	3.6	0.19	2.03	34.1	63	3.4	0.20	1.64
			-30	33.6	56	3.4	0.33	5.48	33.7	57	3.2	0.32	6.29
	0.45	0.6	-30	29.0	54	5.9	0.43	6.45	29.1	55	5.6	0.43	8.30
		1.0	0	33.8	60	3.6	0.20	2.33	34.1	63	3.4	0.20	1.76
			-30	33.6	56	3.4	0.30	6.64	33.7	57	3.2	0.30	6.83
	0.50	0.6	-30	29.3	58	5.9	0.37	6.12	29.5	61	5.3	0.33	8.11
		1.0	0	34.0	62	3.5	0.15	1.99	34.2	65	3.4	0.16	1.57
			-30	33.7	58	3.4	0.30	6.34	33.8	59	3.2	0.30	6.99

In general, the results show excellent performance regardless of the detailed design. Figure 5 summarizes some of the results at 1 GHz from this table. Although

there is absolutely no basis for it, $\bar{\epsilon}$ and $\overline{\langle 0\text{dBi} \rangle}$ (the average of the two gridding schemes) will be used as nominal values for plotting.

One should be somewhat reluctant to draw too strong of a conclusion based on these data, since the percent difference is quite small between the various designs. In fact, the primary conclusion is that it doesn't really matter what you choose within these refinements. However, some tentative conclusions may be drawn. The "blocked" version ($y_c/D=0.45$) seems to exhibit slightly higher efficiencies, however it shows more spillover in the out-of-focus case. Furthermore, the slight blockage in this case is not modeled here. The "flush" version ($y_c/D=0.5$) has the next best ϵ and seems to do best with regard to spillover. The "separated" version ($y_c/D=0.55$) seems to do the worst on nearly all counts. The efficiencies for the out-of-focus case do improve with f/D , as expected; however, the spillover performance doesn't seem to improve and may be slightly degraded. It therefore appears that an antenna with $0.45 \leq y_c/D \leq 0.5$ and $0.4 \leq f/D \leq 0.5$ seems best, with the specific choice being of less importance. The final configuration should therefore be driven by mechanical considerations within these ranges. Figure 6 compares the relevant geometries for $f/D=0.4$ and $f/D=0.5$. Given the size and curvature, an f/D between 0.40 – 0.45 seems warranted.

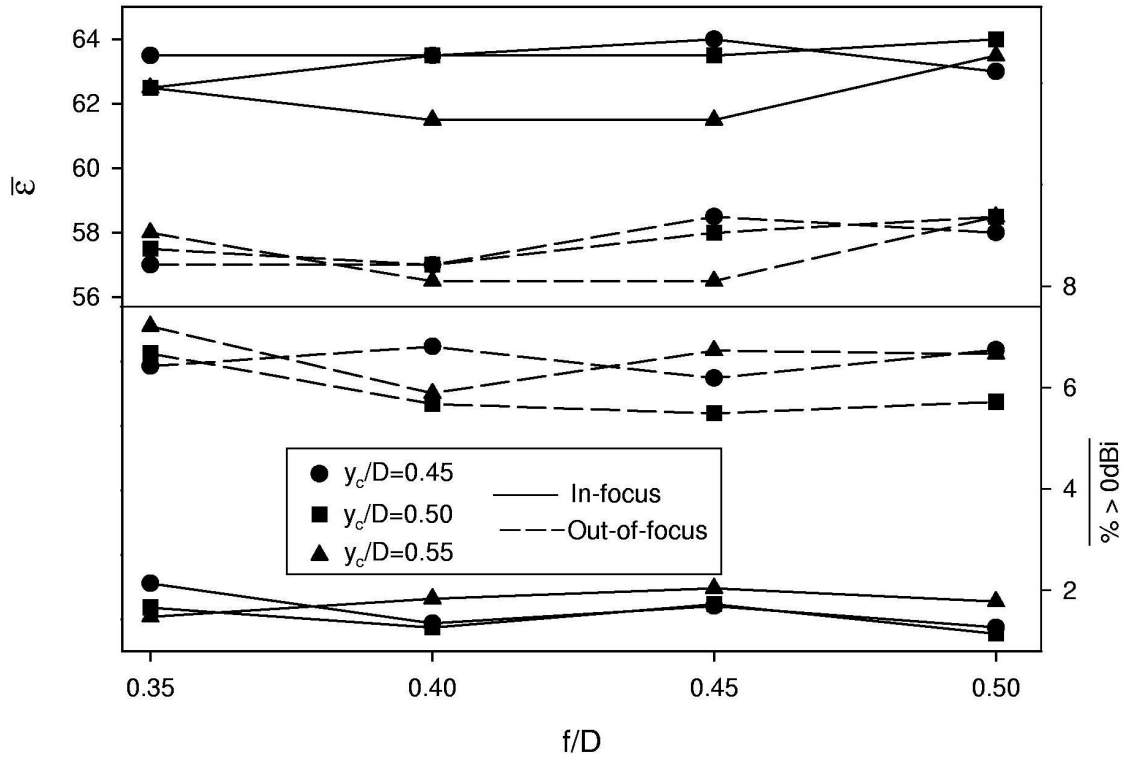


Figure 5: Results at 1 GHz from Table I.

Two Strawman Designs

Given the above analysis, two strawman “flush” designs with $f/D=0.40$ and $f/D=0.45$ are further investigated. Figures 7 and 8 show the detailed co- and cross-polarization patterns in the principal plane for both the in-focus and out-of-focus cases for the two antennas at 1 GHz. Figure 9 shows the sidelobe distributions for the antennas as a cumulative distribution function with the median line indicated. Figure 10 plots the two antennas near boresight to display the inner sidelobes. Figure 11 and 12 show the azimuthally averaged beam pattern at 1 and 3 GHz for $f/D=0.4$, $y_c/D=0.5$.

Table II lists further details of the two strawman designs. G_f is the forward boresight gain while the other columns list the level of the first sidelobe in dB below boresight and the median and 95%ile sidelobe levels in dBi. Table III lists the directivity and median and 95%ile sidelobe levels of the cross-polarized beam and Table IV lists the calculated performance at 3 GHz.

Based on these figures and tables, it is again seen that the impact of choosing either $f/D=0.40$ or 0.45 and $y_c/D=0.45$ or 0.50 is somewhat negligible and should be decided to optimize mechanical considerations, if desired.

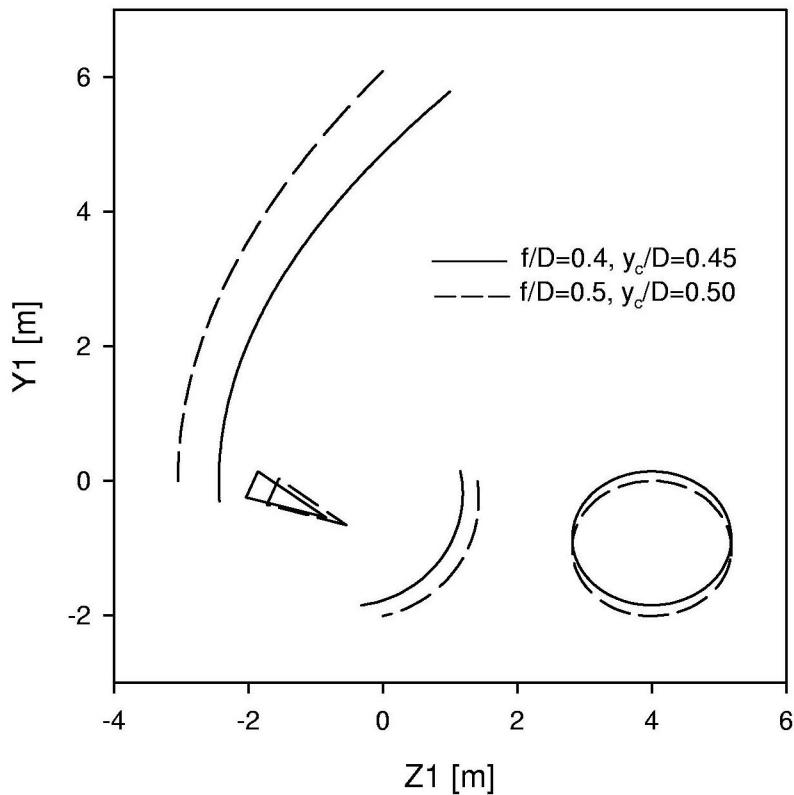


Figure 6: Geometries for two antennas with $y_c/D = 0.50$.

Table II: Further values for $y_c/D=0.5$ antenna designs at 1 GHz.

f/D	Focus [cm]	G_f [dBi]	1 st SLL [dB]	Median SLL [dBi]	95%ile SLL [dBi]
0.40	0	34.36	-21.44	-8.56	-1.64
	-30	33.86	-18.53	-7.28	0.39
0.45	0	34.42	-21.33	-8.15	-1.31
	-30	33.90	-18.98	-6.83	0.42

Table III: Some cross-polarization properties of the two antennas at 1 GHz.

	f/D = 0.40		f/D=0.45	
	In-focus	Out-of-focus	In-focus	Out-of-focus
G_o	20.0	16.2	20.2	15.6
Median	-15.7	-13.2	-14.8	-13.2
95%ile	-6.2	-3.2	-6.1	-2.7

Conclusion

The performance of a set of offset Gregorian antennas has been investigated for use as the ATA antenna design. In general, this unblocked design works exceptionally well. The relative performance of the different antennas is fairly negligible within the limited parameter space that was appropriate. It appears however that an antenna with $0.45 \leq y_c/D \leq 0.50$ with an f/D bounded by $0.40 \leq f/D \leq 0.45$ would provide a good design for the ATA antenna.

One strong caveat on the detailed values presented above in this memo is that the exact diffraction implementation is still somewhat uncertain. You may note that the performance at 600 MHz may seem overly optimistic based on rule-of-thumb application of diffraction with a $\sim \lambda/5$ sub-reflector. I will continue to pursue this with the vendor, and, if necessary, modify the tables and figures above and redistribute. I hope to come to closure on this soon. However, I don't expect the *relative* performance at 1 GHz to vary significantly.

References

- [1] Mizugutch, Y., M. Akagawa and H. Yokoi, "Offset Dual Reflector Antennas", IEEE AP-S Int Symp. Digest, Oct 1976.
- [2] Rusch, W., A. Prata, Y. Rahmat-Samii and R. Shore, "Derivation and Application of the Equivalent Paraboloid for Classical Offset Cassagrain and Gregorian Antennas", IEEE Trans. Ant & Prop vol. 38, pp. 1141-1149, August 1990.

[3] Tanaka, H. and M. Mizusawa, "Elimination of Cross-Polarization in Offset Dual Reflector Antennas", Trans. IECE, Vol 58-B, 1975.

[4] Sletten, C. J. (ed), "Reflector and Lens Antennas: Analysis and Design Using Personal Computers", Artech House, 1988.

[5] Rudduck, R. C. and Y. C. Chang, "Numerical Electromagnetic Code – Reflector Antenna Code (NEC-REF)", Report 712242-16, The Ohio State University ElectroScience Laboratory, Department of Electrical Engineering.

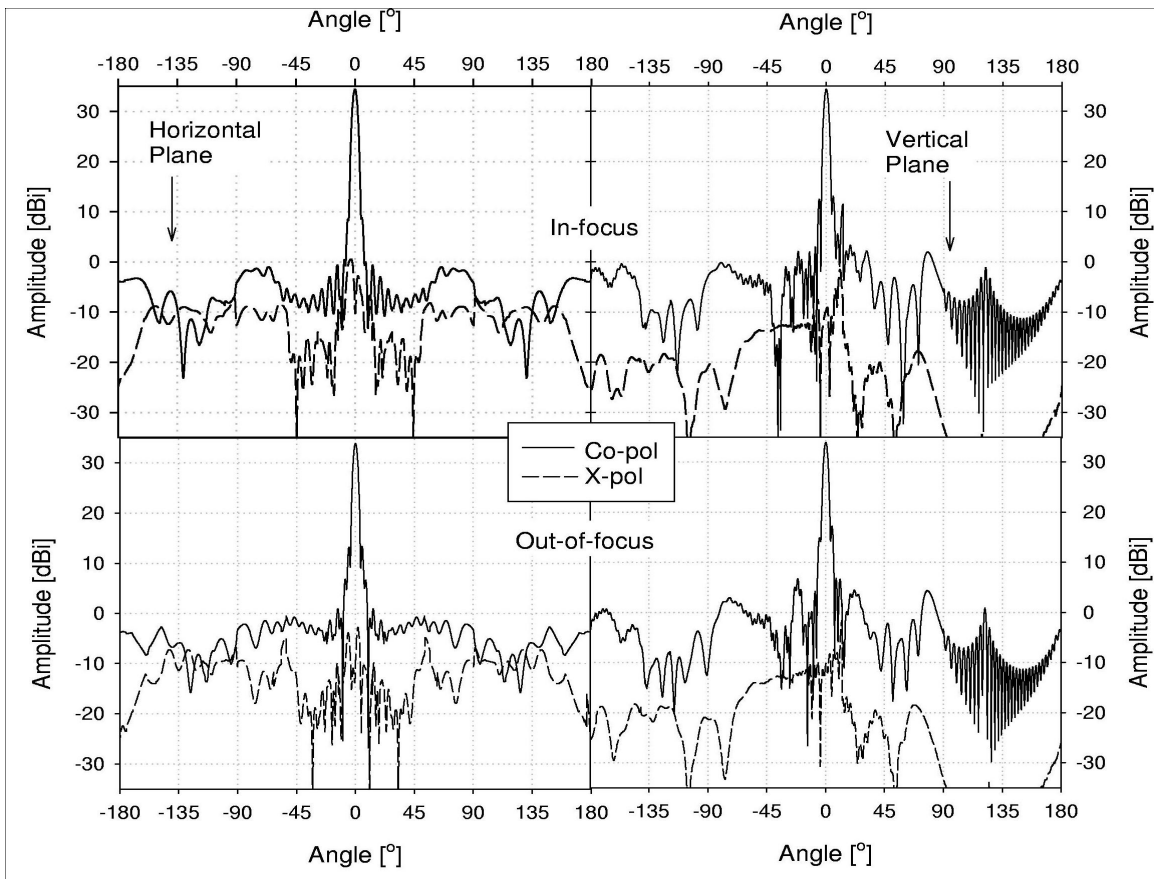


Figure 7: Detailed patterns for $y_c/D=0.50$ and $f/D=0.40$ at 1 GHz.

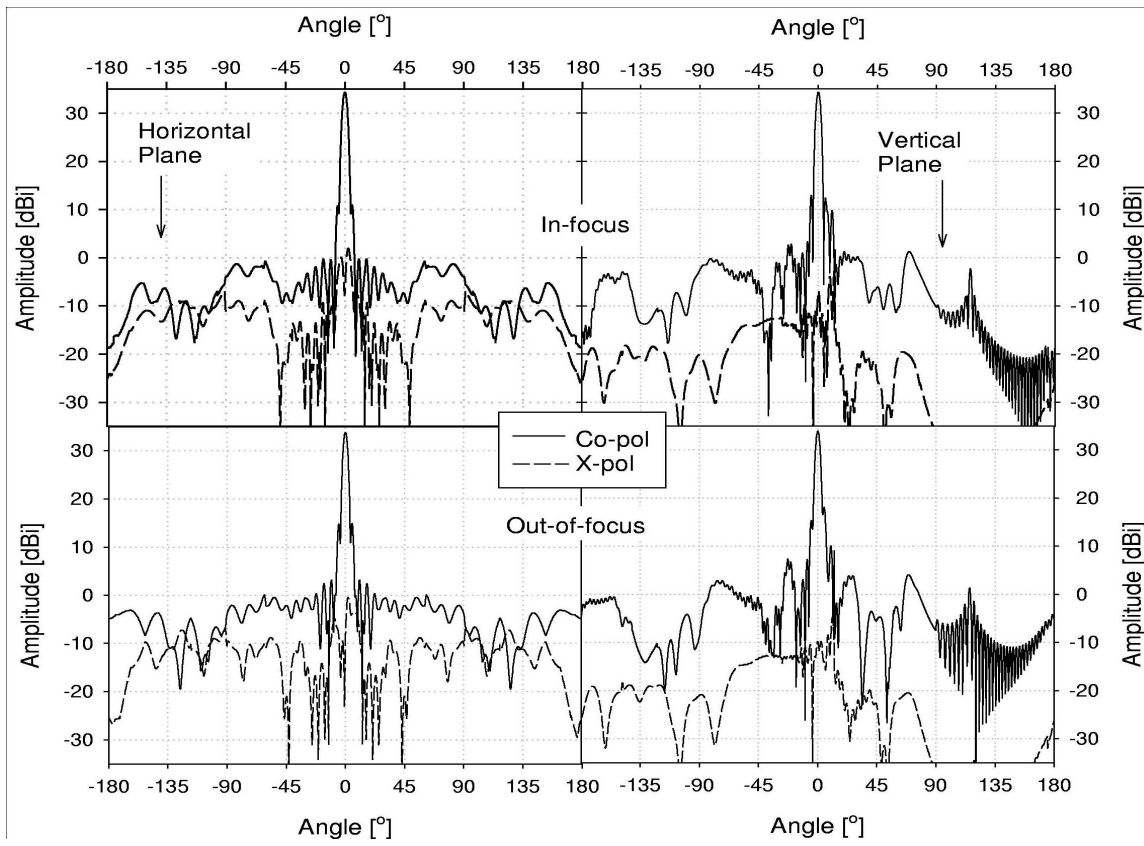


Figure 8: Detailed design with $y_c/D=0.50$ and $f/D=0.45$ at 1 GHz.

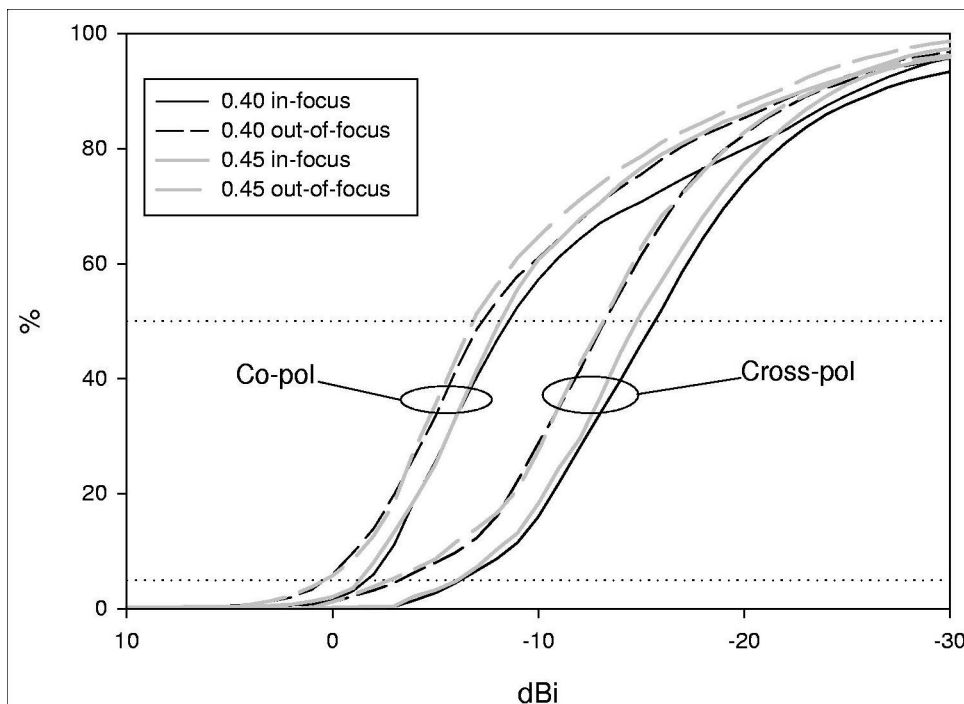


Figure 9: Co- and cross-polarization sidelobe cumulative distribution function for $f/D=0.4$ and $f/D=0.45$.

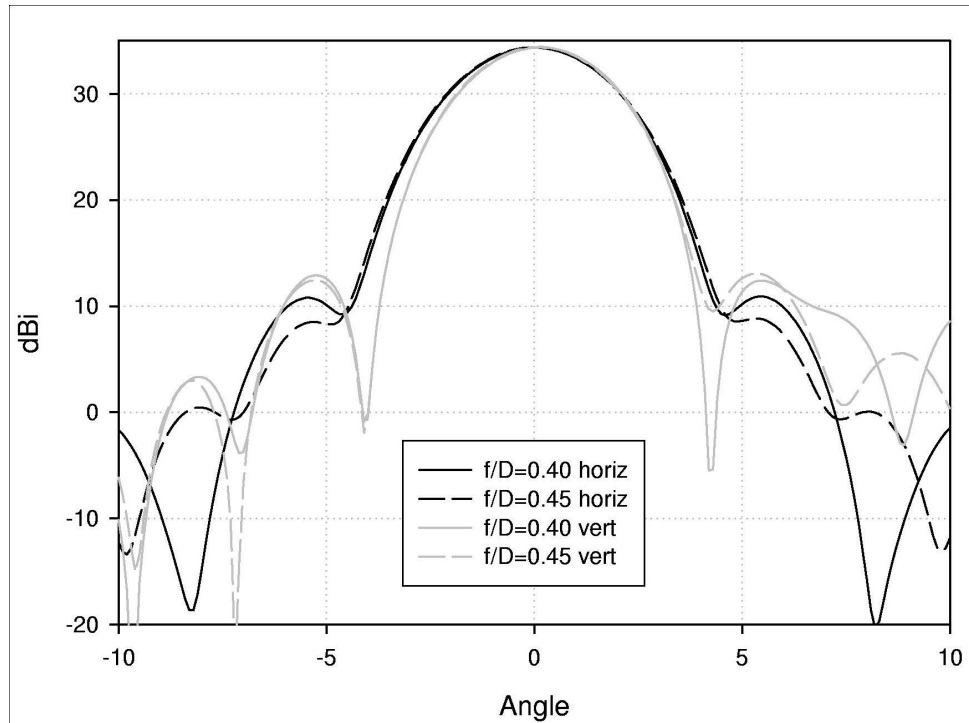


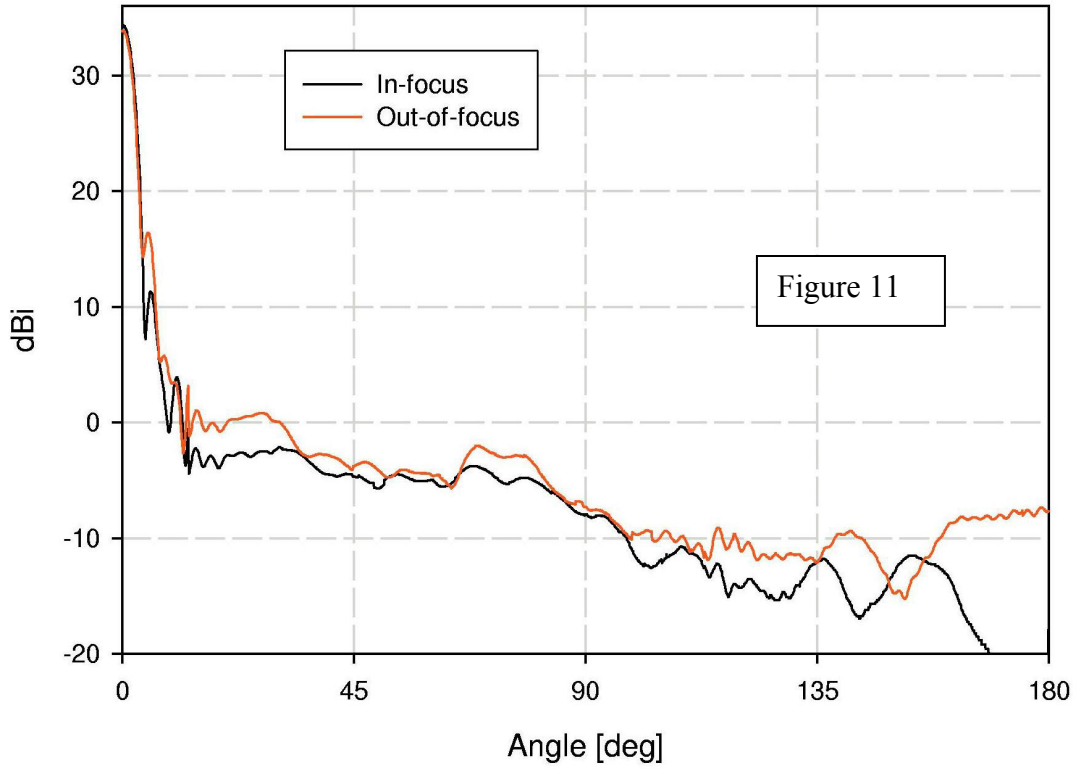
Figure 10: Boresight region for the two antennas in the principal planes at 1 GHz.

Table IV: Antenna performance at 3 GHz.

y_0/D	f/D	Freq [GHz]	Focus [cm] (GHz)	Grid 1					Grid 2				
				G_o [dBi]	ϵ [%]	BW_{3dB}	$>10dBi$	$>0dBi$	G_o [dBi]	ϵ [%]	BW_{3dB}	$>10dBi$	$>0dBi$
						[$^\circ$]	[%]	[%]			[$^\circ$]	[%]	[%]
0.5	0.4	3.0	0	43.9	66	1.15	0.06	1.53	43.9	66	1.12	0.07	1.76
						1.96	-9.07	-1.95			1.93	-8.27	1.58
			+15 (1.42)	41.2	36	1.32	0.10	0.52	41.3	37	1.30	0.10	0.43
						2.90	-10.03	-2.66			2.85	-9.40	-2.30
			-7 (6)	43.7	65	1.13	0.07	2.83	43.7	65	1.10	0.08	3.05
						1.93	-8.65	-1.27			1.90	-7.85	-1.10

Azimuthally-Averaged Antenna Pattern at 1 GHz

$f/D=0.40$ $y_c/D=0.50$



Azimuthally Averaged Beam Pattern at 3 GHz

$f/D = 0.40$ $y_c/D = 0.50$

